JACS
JOURNAL OF THE AMERICAN CHEMICAL SOCIETY

Article

pubs.acs.org/JACS

Triple Helix Formation in Amphiphilic Discotics: Demystifying Solvent Effects in Supramolecular Self-Assembly

Martijn A. J. Gillissen, Marcel M. E. Koenigs, Jolanda J. H. Spiering, Jef A. J. M. Vekemans, Anja R. A. Palmans,* Ilja K. Voets, and E. W. Meijer*

Institute of Complex Molecular Systems, Laboratory of Macromolecular and Organic Chemistry, Eindhoven University of Technology, P.O. Box 513, 5600 MB, Eindhoven, The Netherlands

Supporting Information

ABSTRACT: A set of chiral, amphiphilic, self-assembling discotic molecules based on the 3,3′-bis(acylamino)-2,2′-bipyridine-substituted benzene-1,3,5-tricarboxamide motif (BiPy-BTA) was prepared. Amphiphilicity was induced into the discotic molecules by an asymmetrical distribution of alkyl and oligo(ethylene oxide) groups in the periphery of the molecules. Small-angle X-ray scattering, cryogenic transmission electron microscopy, and circular dichroism spectroscopy measurements were performed on the discotic amphiphiles in mixtures of water and alcohol at temperatures between 0 °C an 90 °C. The combined results show that these amphiphilic discotic molecules self-assemble into supramolecular fibers consisting of either one or three discotic molecules in the fiber cross-section and that the presence of water induces the bundling of the supramolecular fibers. The rich phase behavior observed for these molecules proves to be intimately connected to the mixing thermodynamics of the water−alcohol mixtures.

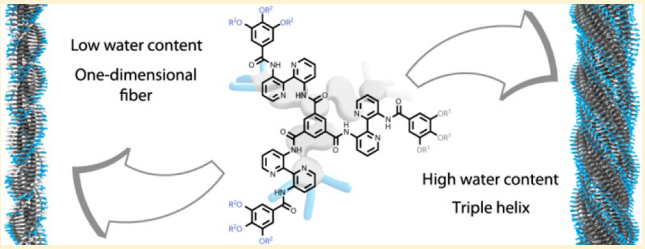

INTRODUCTION

The self-assembly of molecular components is an intriguing, low-energy pathway toward materials with nanoscopic order.[1] A widely studied class of self-assembling molecules consists of disc-shaped molecules that form one-dimensional (1D) fibers.[2−4] The creation of more complex superstructures with advanced functionality requires not only control over the assembly of molecules into 1D fibers but also control over the next step, assembly of fibers into bundles or fibrils. Such bundled structures occur frequently in natural proteins and have also been realized in synthetic proteins and peptides.[5] The leucine zipper[6] structural motif and the tropomyosin coiled coil[7] are stabilized to a large extent by hydrophobic interactions,[8] while other naturally occurring structures such as the collagen triple helix[9] are held together mainly by hydrogen-bonding interactions. Inspired by the coiled-coils, double and triple helices found in nature, chemists successfully developed several elegant approaches toward these architectures from fully synthetic building blocks in organic media.[10−31] Driven by the potential of self-assembled materials in biomedical applications, much current research is focused on developing fully synthetic systems that form fibrillar structures in aqueous media.[32−36] Translating the design rules for self-assembly in apolar organic solvents to water is not trivial, as additional factors, such as the hydrophobic effect and interference of water with hydrogen bonding interactions, start playing a role. In addition, to help compatibilize synthetic self-assembling systems with water, a cosolvent is frequently added, resulting in self-assembly behavior that is not necessarily predictable.[37−42]

We here illustrate how the self-assembly behavior in water of an amphiphilic discotic molecule, encoded to form bundled structures by incorporating two orthogonal interactions, is affected by mixing water and an alcohol. We select the 3,3′-bis(acylamino)-2,2′-bipyridine-substituted benzene-1,3,5-tricarboxamide discotic (BiPy-BTA), which is known to self-assemble into 1D helical fibers in apolar and polar organic solvents and even in water, due to $\pi-\pi$ interactions.[43−49] In addition, the BiPy-BTA discotic is robust to modification of its periphery. The amphiphilicity of the molecule is induced by placing alkoxy groups on the three R^1 positions and oligo(ethylene oxide) groups on the six R^2 positions, thus incorporating the hydrophobic effect as an orthogonal interaction (Figure 1). Breaking the C_3 symmetry of the BiPy-BTA discotic facilitates the hierarchical self-assembly into bundled structures. To introduce a preference for a single helical handedness, we incorporate chiral alkyl or oligo(ethylene oxide) side chains. This strategy results in the formation of 1D helical fibers in pure isopropanol, when only the $\pi-\pi$ interactions are operative, while triple helical bundles are formed in isopropanol−water (IPA−H_2O) mixtures, in which the hydrophobic effect starts playing a role. A detailed study of the self-assembly as a function of solvent composition and temperature reveals that the solvent drives the observed morphological transitions, as suggested by Trappe and co-workers for poly(*N*-isopropylacrylamide) in water−alcohol mixtures.[50] We observe three distinct structural regimes with

Received: October 10, 2013
Published: December 7, 2013

dx.doi.org/10.1021/ja4104183 | *J. Am. Chem. Soc.* 2014, 136, 336−343

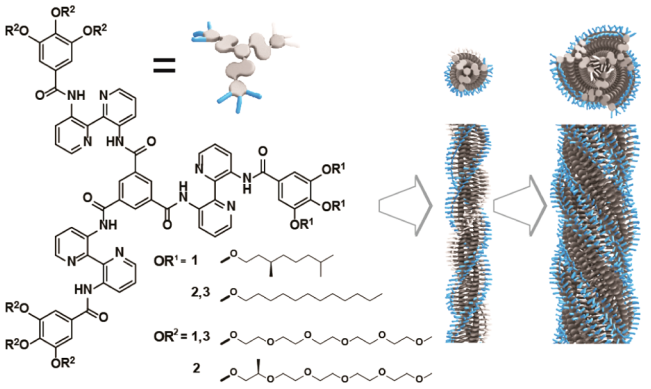

Figure 1. Chemical structure of amphiphilic BiPy-BTA discotics **1**−**3** and their hierarchical self-assembly, first into a supramolecular fiber and then into a triple helical bundle.

boundaries that coincide with the extrema in the excess enthalpy of mixing (ΔH_{mix}^{E}) of IPA−H_2O mixtures.

RESULTS AND DISCUSSION

Synthesis of Compounds 1−3. Compounds **1**−**3** were synthesized in a stepwise approach (Scheme 1) starting from 5-(methoxycarbonyl)benzene-1,3-dicarboxylic acid (**4**).[51] In the initial step, the diacid was converted to the diacid dichloride using oxalyl chloride, after which it was coupled to the bipyridine monoamines **5a** or **5b** that contain water-soluble oligo(ethylene oxide) chains. The obtained monoesters **6a** and **6b** were then saponified using lithium hydroxide at 85 °C and subsequently neutralized with oxalic acid. In the final step, the monoacids **7a** and **7b** were converted into the acid chloride using Ghosez's reagent[52] and coupled to the alkyl-decorated bipyridines **8a**,**b** to obtain the final products **1**−**3**. All end-products were analyzed by ^{1}H and ^{13}C NMR, MALDI−TOF MS, and elemental analysis; the results were consistent with the proposed structures (see Supporting Information section 3 for details of the synthesis).

Characterization of Compounds 1−3. A combination of spectroscopic, microscopic, and scattering techniques was applied to investigate how solvent composition, temperature, and concentration affect the supramolecular structures formed upon self-assembly of compound **1**. Circular dichroism (CD) experiments were performed as a function of the volume fraction of isopropanol (ϕ_{IPA}), temperature, and concentration to investigate under which conditions **1** self-assembles. The shape and size of the supramolecular structures obtained were subsequently investigated by cryogenic transmission electron microscopy (cryo-TEM) and small-angle X-ray scattering (SAXS). This combination of experimental techniques reveals that solvent composition and temperature determine the nature of the aggregates, and three distinct regimes can be distinguished. The results are discussed in detail below.

Circular Dichroism Spectroscopy. CD spectra of **1** were measured in IPA−H_2O mixtures at 0 °C. The volume fraction of isopropanol (ϕ_{IPA}) was 1, 0.5, or 0.25 and the concentration of **1** was constant at 3×10^{-4} M. In all solvent mixtures, Cotton effects were observed, indicating the presence of helical objects of one predominant handedness (Figure 2). However, the shape of the CD spectra differs considerably between the three solvent compositions.

At $\phi_{IPA} = 1$, the CD spectrum shows minima at λ = 235, 286, 367, and 385 nm, with a molar circular dichroism ($\Delta\varepsilon$) at 286 nm of −39 L mol^{-1} cm^{-1} (Figure 2F). The Cotton effect has a shape and magnitude similar to those previously observed for symmetrical, aliphatic BiPy-BTA compounds in apolar organic solvents.[46] At $\phi_{IPA} = 0.5$, the Cotton effect shows a maximum at λ = 335 nm ($\Delta\varepsilon$ = 119 L mol^{-1} cm^{-1}) and minima at λ = 263 and 302 nm (Figure 2E). Finally at ϕ_{IPA} = 0.25 we find a Cotton effect with a maximum at λ = 310 nm ($\Delta\varepsilon$ = 39 L mol^{-1} cm^{-1}) and minima at λ = 235, 283, and 385 nm shown in Figure 2D. These observations show that whereas **1** forms

Scheme 1. Synthesis of Amphiphilic BiPy-BTA Discotics 1−3

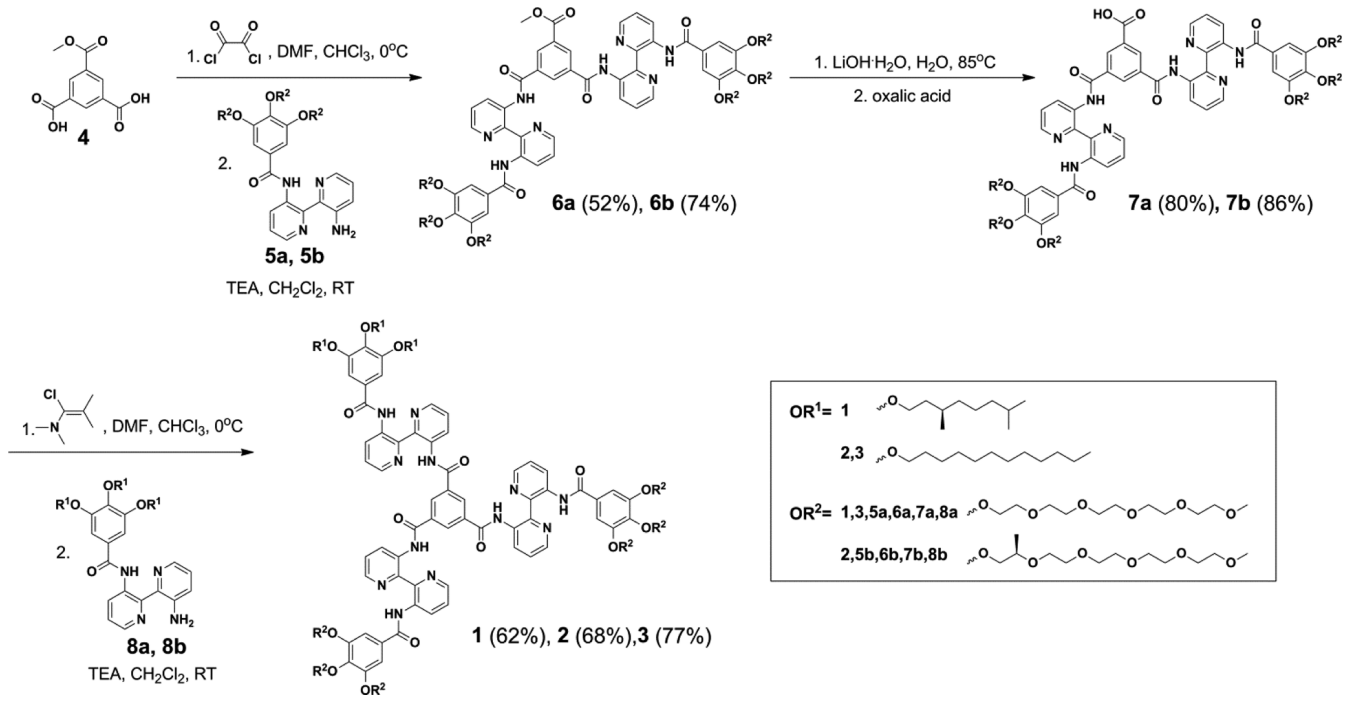

dx.doi.org/10.1021/ja4104183 | J. Am. Chem. Soc. 2014, 136, 336−343

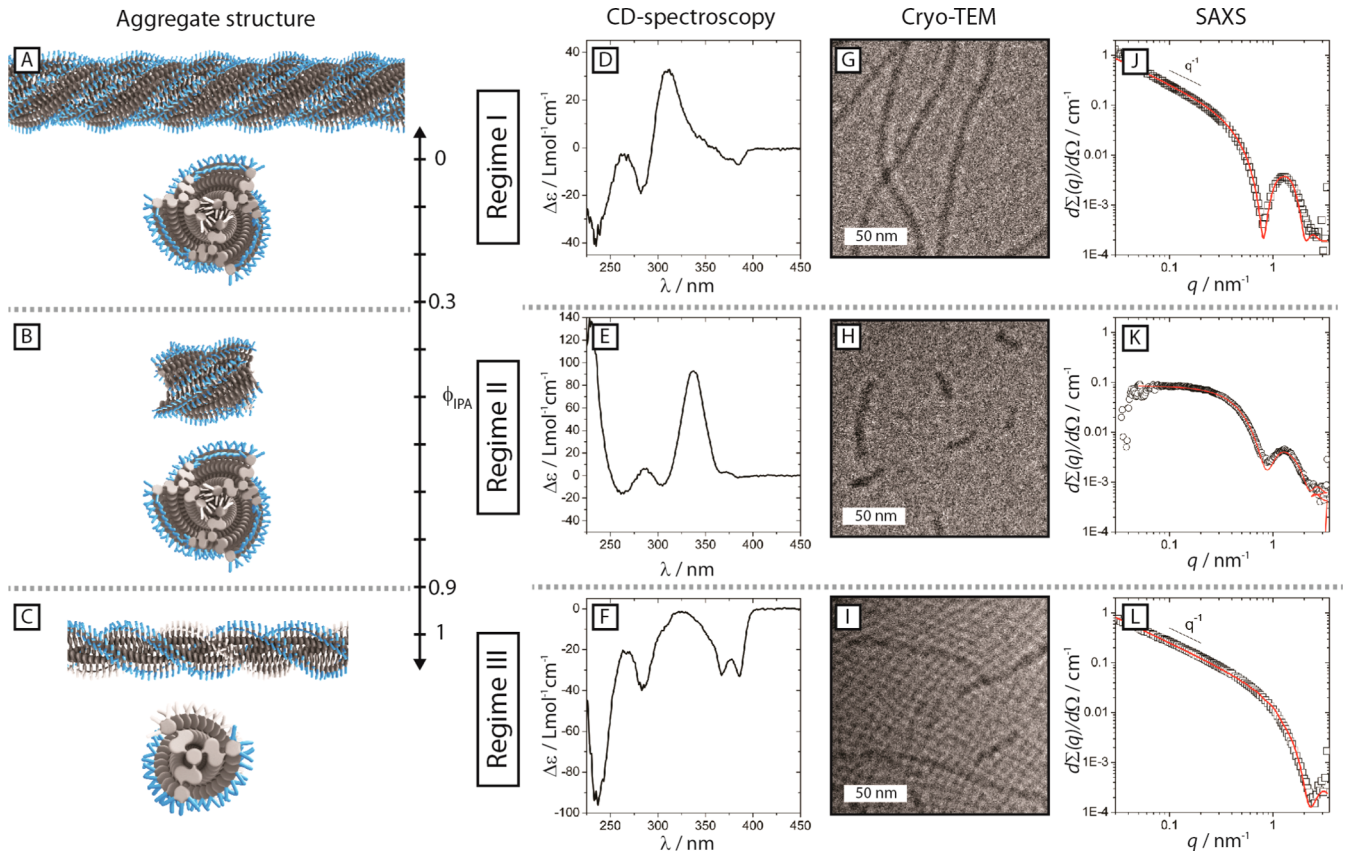

Figure 2. (A–C) Schematic depiction of the three regimes in self-assembly of **1** in IPA–H_2O. CD-spectra of **1** at $c = 3 \times 10^{-4}$ M and $T = 0$ °C for (D) $\phi_{IPA} = 0.25$, (E) $\phi_{IPA} = 0.5$, and (F) $\phi_{IPA} = 1$. Cryo-TEM images of **1** at $c = 3 \times 10^{-4}$ M for (G) $\phi_{IPA} = 0.25$, (H) $\phi_{IPA} = 0.75$, and (I) $\phi_{IPA} = 1$. SAXS profiles (symbols) and form factor fits (lines) for **1** in IPA–H_2O mixtures at $c = 3 \times 10^{-4}$ M and $T = 20$ °C for (J) $\phi_{IPA} = 0.25$, (K) $\phi_{IPA} = 0.5$, and (L) $\phi_{IPA} = 1$.

chiral aggregates in all solvent mixtures, the arrangement of the discotic molecules inside the aggregates is strongly determined by the solvent composition.

To study the influence of temperature on the formation of self-assembled structures of **1**, we performed temperature-dependent CD experiments. In all cases, the solutions of **1** were cooled from 80 °C to 0 °C and the CD effect was monitored at one specific wavelength (Figure S1, Supporting Information). In pure isopropanol ($\phi_{IPA} = 1$), a sigmoidal temperature-dependence of the Cotton effect is observed when monitoring $\Delta\varepsilon$ at 286 nm (Figure 3A). Such sigmoidal curves are indicative for an isodesmic self-assembly mechanism.[53] The temperature-dependent cooling curves were fit to an isodesmic model, which allows quantification of the melting temperature (T_m) and the enthalpy release for bond formation (ΔH) summarized in Figure 4 and Table S1 (see Supporting Information section 4 for details). At a concentration of 3×10^{-4} M and at $\phi_{IPA} = 1$, $\Delta H = -142$ kJ mol^{-1} and $T_m = 328$ K. Upon decreasing the concentration of **1** in IPA, T_m shifts to lower temperatures while ΔH remains rather constant.

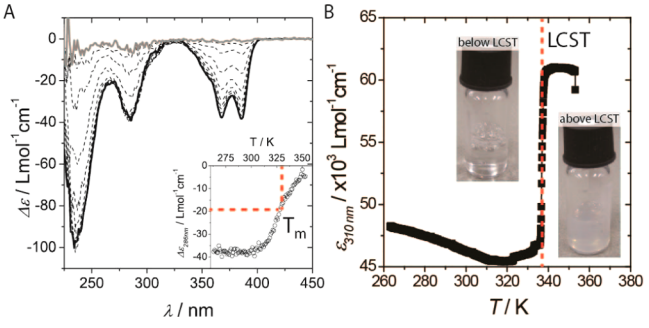

Figure 3. (A) Temperature-dependent CD spectra for **1** at $c = 3 \times 10^{-4}$ M and $T = 80$ to -10 °C in $\phi_{IPA} = 1$. (B) UV heating curve monitored at $\lambda = 310$ nm for **1** at $c = 3 \times 10^{-5}$ M in $\phi_{IPA} = 0.1$.

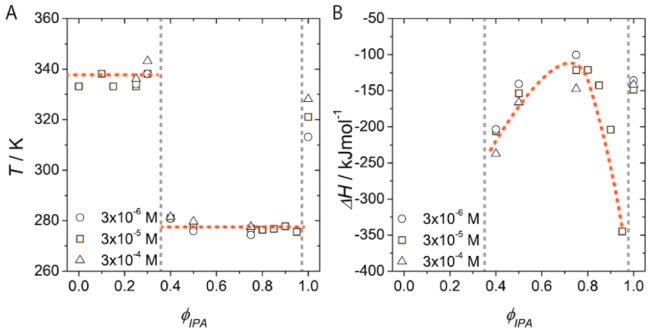

Figure 4. (A) Transition temperature (T_m or LCST) for compound **1** in regimes I, II, and III in IPA–H_2O mixtures. (B) Enthalpy release upon bond formation (ΔH) for compound **1** in regimes I, II, and III in IPA–H_2O mixtures.

In the range of $0.4 \leq \phi_{IPA} \leq 0.9$, the CD spectra are similar to those observed at $\phi_{IPA} = 0.5$. In addition, monitoring $\Delta\varepsilon$ at 340 nm as a function of temperature in the range of $0.4 \leq \phi_{IPA} \leq 0.9$ shows a sigmoidal temperature-dependence of the CD-

dx.doi.org/10.1021/ja4104183 | J. Am. Chem. Soc. 2014, 136, 336–343

effect (Figure 3B). The melting temperatures (T_m) for these solvent compositions are substantially lower than that observed in pure isopropanol. For example, at a concentration of 3×10^{-4} M and at $\phi_{IPA} = 0.5$, T_m is 280 K with a corresponding ΔH of −166 kJ mol^{-1}. The T_m does not change strongly with ϕ_{IPA} or the concentration of **1**. The ΔH, on the other hand, has a strong nonlinear dependence on ϕ_{IPA}.

At $\phi_{IPA} \leq 0.3$, the CD spectrum changes shape, and temperature-dependent CD experiments reveal that the magnitude of the CD-effects hardly changes with increasing temperature. The UV trace of the cooling curve shows an abrupt increase in intensity above ca. 340 K, indicative of a lower critical solution temperature (LCST) as shown in Figure 3B. The temperature of the LCST transition is virtually independent of the BiPy-BTA concentration and ϕ_{IPA} as shown in Figure 4A.

Cryogenic Transmission Electron Microscopy. The structures of the aggregates formed by **1** in IPA−H_2O mixtures at a concentration of 3×10^{-4} M were visualized by cryo-TEM (Figure S3, Supporting Information). These experiments reveal a remarkable difference in aggregate structure upon changing the solvent composition from pure IPA to predominantly water. In pure isopropanol (Figure 2I), long, fibrous objects are present. The length of these aggregates ranges from 100 to several 100 nm. In contrast, the cross-section of the fibers is constant with a diameter of approximately 7 nm. At intermediate isopropanol content, $\phi_{IPA} = 0.75$ (Figure 2H), low aspect ratio objects are observed. The length of these aggregates ranges from 10 to 50 nm, whereas the cross-section is constant at approximately 10 nm. Finally, at low isopropanol content, $\phi_{IPA} = 0.25$ (Figure 2G), we observe very long fibrous objects with lengths of several micrometers. The cross-section is constant at approximately 11 nm. It should be noted that contrast, resolution, and focusing issues hamper a more exact determination of the dimensions of the cross-section.

Small Angle X-ray Scattering. The aggregate structure of **1** in IPA−H_2O mixtures at a concentration of 3×10^{-4} M was studied in more detail by SAXS. The scattering profiles are shown in Figures 5A, and Figures S4 and S5 (Supporting Information). At high and low ϕ_{IPA} the scattering profiles at low q values exhibit power law scaling behavior, $I \propto q^{-1}$, indicative of rigid objects elongated in one dimension with a length beyond the experimentally probed q range. At the intermediate solvent compositions we see a $I \propto q^0$ dependence of the scattered intensity at low q, typical for low aspect ratio objects with a length within the experimentally probed q range. At high q values, form factor oscillations are observed, indicating the presence of a well-defined cross-section. The position of the first minimum is significantly different for high and low ϕ_{IPA}, indicating a significant difference in cross-section dimensions in these two regions. We applied two methods to collect information on the dimensions of the self-assembled objects, the indirect Fourier transform (IFT), and form factor analysis.

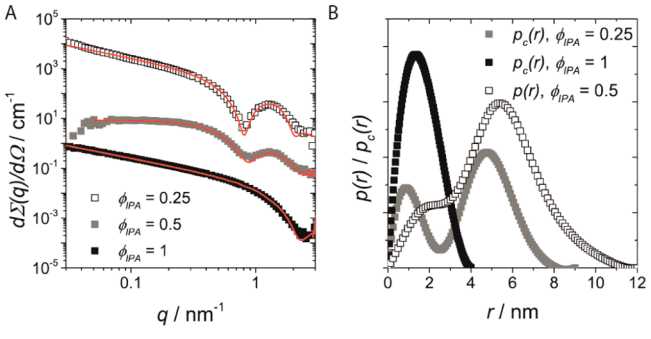

Figure 5. SAXS data for **1** in IPA−H_2O mixtures at $c = 3 \times 10^{-4}$ M and T = 20 °C: (A) SAXS profiles (symbols) and form factor fits (lines) (data is offset by a factor of 10^2 ($\phi_{IPA} = 0.5$) and 10^4 ($\phi_{IPA} = 0.25$) for clarity). (B) Cross-sectional PDDFs and PDDFs for $\phi_{IPA} = 1$, 0.25, and 0.5.

The IFT is a model-independent method to obtain information on the scattering object by generating a pair distance distribution function (PDDF, $p(r)$) of the scattering particle.[54] This PDDF gives the probability of finding a point at a distance r starting from a random point within the particle, weighed by the difference in electron density between these two points if it is not constant over the whole particle. Therefore, the maximal dimension of a particle corresponds to the maximal distance (r) of the PDDF, where $p(r) \neq 0$. The PDDF typically exhibits one or several peaks at distances characteristic for the object studied. For example, in the case of a sphere, this maximum occurs approximately at the radius. In the case of objects that are elongated in one dimension, a PDDF of the cross-section can be determined ($p_c(r)$). Figure 5B and Figure S4 (Supporting Information) show the obtained $p_c(r)$ and $p(r)$. The $p_c(r)$ of the aggregate in pure isopropanol is a single Gaussian-like peak with a maximum at r = 1.3 nm, extending to r = 4 nm (Figure 5B). This shape is typical for an object having a circular cross-section with one fixed scattering length density (ρ) over the entire cross-section.[54] However, at ϕ_{IPA} = 0.25 and 0.3, the $p_c(r)$ of the aggregate show two maxima at r = 0.9 and 4.8 nm, extending to r = 7.5 nm. This shape is typical for an object having two distinct scattering length densities along the cross-section, i.e., a core−shell object.[54] Finally, at the intermediate solvent compositions, the $p(r)$ show two maxima at r = 2.1 and 5.5 nm, extending to r = 8, 12, and 18 nm for ϕ_{IPA} = 0.75, 0.5 and 0.4, respectively (Figures 5B and Figure S4, Supporting Information). These PDDFs are typical for objects having a core−shell structure where the length of the objects becomes larger going from ϕ_{IPA} = 0.75 to 0.4.

The PDDFs show that aggregates of **1** can be described as objects elongated along one direction, which at $\phi_{IPA} < 1$ have a core−shell cross-section and at $\phi_{IPA} = 1$ have a cross-section with only a core (without a shell). This can be depicted as a (core−shell) cylinder having a length (L), a (core) radius (R), and a shell thickness (T), each having their own scattering length density (ρ) depicted in Figure 6.

To further quantify the dimensions of the aggregates, the SAXS profiles were fit to a model for either a cylinder (cyl) or a core−shell cylinder (cs−cyl). The SAXS profiles and form factor fits are shown in Figures 5A and Figures S4 and S5 (Supporting Information), and the extracted aggregate dimensions are given in Table 1 and Table S3 (Supporting Information). At high and low isopropanol contents, where the q^{-1} power law scaling of the scattered intensity is observed, the aggregates are too long to determine their length by the SAXS experiments, and these are therefore set at 1000 nm. In pure isopropanol the aggregates have a radius (R) of ca. 1.65 nm, having a homogeneous scattering length density (ρ) over the whole cross-section. Experiments at ϕ_{IPA} = 0.3 and 0.25 reveal that the aggregates have an inhomogeneous ρ over the cross-section, i.e., a core−shell structure, with an inner radius (R) of ca. 1.5 nm and an outer radius ($R+T$) of ca. 3.5 nm. At intermediate isopropanol contents, the length of the aggregates

dx.doi.org/10.1021/ja4104183 | J. Am. Chem. Soc. 2014, 136, 336−343

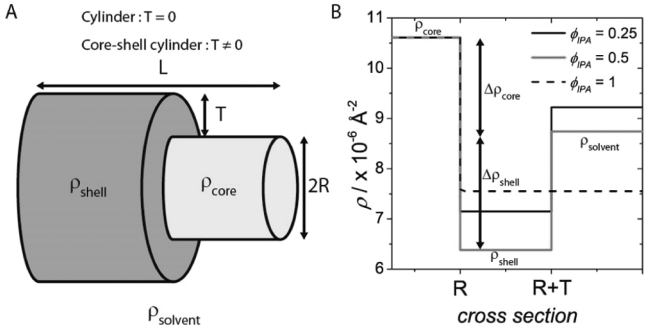

Figure 6. (A) Schematic depiction of a cylinder and core−shell cylinder model. (B) Depiction of scattering length density (ρ) along the cylinder cross-section and contrast ($\Delta\rho$) of core and shell for ϕ_{IPA} = 0.5 (arrows).

Table 1. Fit Parameters Obtained from Form Factor Fits to SAXS Profiles of Compound 1 in IPA−H_2O Mixtures, Where *L* = Cylinder Length, *R* = Core Cross-Section, and *T* = Shell Thickness

		dimensions (nm)		
ϕ_{IPA}	regime	*L*	*R*	*T*
1	III	1000[a]	1.7 ± 0.1	–
0.75	II	8.5 ± 1.7	1.4 ± 0.1	–
0.5	II	5.1 ± 0.7	1.6 ± 0.2	1.7 ± 0.3
0.4	II	13.8 ± 2.0	1.6 ± 0.1	1.8 ± 0.2
0.3	I	1000[a]	1.4 ± 0.1	2.3 ± 0.2
0.25	I	1000[a]	1.6 ± 0.1	2.1 ± 0.2

[a]This value was set as fixed in the fitting procedure.

falls within the experimentally probed range. Here, we observe the presence of low aspect ratio objects, with an average length of 5 to 15 nm. In all cases an inner radius of ca. 1.5 nm is determined. Where for ϕ_{IPA} = 0.4 and 0.5 an outer radius of ca. 3.2 nm is observed, no shell contrast is seen for ϕ_{IPA} = 0.75. The latter observation could be caused by the change in shell contrast ($\Delta\rho_{shell}$), which is the scattering length density difference between the shell and the surrounding solvent, gradually diminishing the "visibility" of the shell (Figure 6B).

Overall we observe that the fiber radius in the regime where core−shell structures are formed is approximately twice that observed for fibers in pure isopropanol. The latter is consistent with bundle formation of the smaller isopropanol regime fibers into bundles of 3 to 4 fibers. This observation is further substantiated by calculation of the mass per unit length (M_L) of the aggregates from the SAXS profiles. With this information we can estimate the number of discotic molecules in the cross-section of the aggregate (Table S5, Supporting Information). Whereas the cross-section at ϕ_{IPA} = 1 contains one discotic molecule, the ϕ_{IPA} = 0.25 aggregate consists of three discotic molecules.

To summarize, the SAXS experiments corroborate the ϕ_{IPA} dependence of aggregate length apparent in the cryo-TEM images. Whereas at high and low isopropanol content long fibers are present, in the intermediate regime low aspect ratio objects are observed. The SAXS experiments give additional information on the cross-section of the observed fibers. The increased diameter of the fibers upon addition of water is pointing to the formation of a core−shell structure of the cross-section. We propose that the observed core−shell cross-section is the result of bundling of three 1D fibers into a coiled superstructure, in which the aliphatic substituents cluster in the center of the fiber. This separation of aliphatic and ethylene oxide chains results in a contrast difference along the fiber cross-section. It is likely that the addition of water will cause the helical aggregates to assemble in such a way that the hydrophobic parts are shielded from the hydrophilic outside. Because the discotics have a flexible propeller shape but are never complete flat, the most likely conformation is a triple helix of helices. In fact, MD calculation performed previously by Amabilino and co-workers[43] on bipyridine-based discotics showed that three primary fibers in an *M* conformation wrap spontaneously one around the other to converge into a coiled superhelix. In our case, with the hydrophobic effect present, such an organization is even more likely.

Three Regimes of Self-Assembly. The above experiments show that we can distinguish three regimes for the self-assembly of compound **1** and in each regime, the structural and mechanistic properties of aggregates formed by **1** differ (Figure 2).

Regime I. In the low isopropanol content regime, at $\phi_{IPA} \leq$ 0.3, we observe long fibrous aggregates having a core−shell cross-section. The aggregates have a preferential chirality and consist of three BiPy-BTA molecules in their cross-section: a triple helical bundle.

Regime II. In the intermediate isopropanol content regime, at 0.4 $\leq\phi_{IPA} \leq$0.9, we observe low aspect ratio objects having a core−shell cross-section and a preferential chirality.

Regime III. In the high isopropanol content regime, at ϕ_{IPA} = 1, we observe long fibrous aggregates having a cross-section with a single, homogeneous contrast. The aggregates have a preferential chirality and consist of one BiPy-BTA molecule in their cross-section: a one−dimensional helical fiber.

The findings discussed above unambiguously demonstrate that the combination of solvent composition and temperature dictate the structure of the supramolecular polymers formed by **1** and their formation mechanism. Inspired by recent work by Trappe and co-workers, who showed that the LCST transition in poly(*N*-isopropylacrylamide) in mixed solvents is correlated to the solvent mixing thermodynamics, we decided to investigate whether such correlation exists in the self-assembly process of compounds **1**−**3**.[50]

Enthalpy of Mixing of IPA and H_2O. We first focus on the (excess) enthalpy of mixing (ΔH_{mix}^{E}) of IPA and H_2O, which is known to be strongly asymmetric in its composition dependence.[55−57] The excess enthalpy of mixing is one of the several properties that reflect the well-documented anomalous properties of many water−alcohol mixtures.[55] The ΔH_{mix}^{E} shows a temperature-dependent minimum at low isopropanol content (ϕ_{min}) and maximum at high isopropanol content (ϕ_{max}). Both ϕ_{min} and ϕ_{max} shift to higher ϕ_{IPA} upon decreasing temperature (Figure 7A).

There is a remarkable correlation between the dependence of the ΔH_{mix}^{E} and regimes I, II, and III on ϕ_{IPA}. At 20 °C, we find the transition from regime I to II ($\phi_{I\rightarrow II}$) at $\phi_{IPA} \sim$ 0.35, a solvent composition almost identical to the minimum $\phi_{min} \sim$ 0.35 in Figure 7A. In addition, the transition from regime II to III ($\phi_{II\rightarrow III}$) is situated at $\phi_{IPA} \sim$ 0.95, which is close to the maximum at $\phi_{max} \sim$ 0.93 in Figure 7A. To test whether the boundary between regime II and III in the self-assembly of compound **1** is indeed coupled to the excess enthalpy of mixing, we performed a temperature-dependent experiment at ϕ_{IPA} = 0.95.

dx.doi.org/10.1021/ja4104183 | J. Am. Chem. Soc. 2014, 136, 336−343

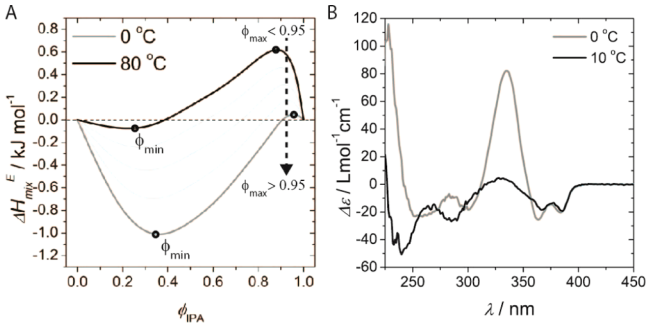

Figure 7. (A) Temperature- and ϕ_{IPA}-dependence of ΔH_{mix}^{E} for IPA–H_2O (figure based on data from refs 38 and 39). (B) Temperature-dependent CD spectra for **1** at $c = 3 \times 10^{-5}$ M in $\phi_{IPA} = 0.95$.

Figure 7A shows that at 80 °C, ϕ_{max} is well below 0.95 while at 0 °C, ϕ_{max} shifts to values larger than 0.95. This would suggest that cooling a solution of **1** in $\phi_{IPA} = 0.95$ should induce a change in the nature of the aggregates typical for regime III to an aggregate typical for regime II. To test this, the CD spectra of a solution of **1** in $\phi_{IPA} = 0.95$ were measured at different temperatures. Figure 7B shows that at 10 °C, a Cotton effect typical for regime III is observed. Upon cooling the solution to 0 °C, the CD-effect changes significantly and is typical for regime II. This clearly shows that the self-assembly of **1** in water–IPA mixtures is intricately linked to the mixing behavior of this solvent mixture.

Changing Cosolvent and Peripheral Substitution. The positions of ϕ_{min} and ϕ_{max} depend not only on temperature but also on the alcohol used as cosolvent. In EtOH–H_2O at 25 °C, ϕ_{min} is ca. 0.4, and there is no maximum in ΔH_{mix}^{E}. At elevated temperatures, there is a maximum at $\phi_{max} \sim 0.77$ at $T = 75$ °C.[55] To further substantiate the relation between the phase behavior of amphiphilic BiPy-BTAs and the extrema of ΔH_{mix}^{E}, we performed experiments on compound **1** in ethanol–water mixtures (EtOH–H_2O). Additionally, we investigated the behavior of BiPy-BTA derivatives **2** and **3** in isopropanol–water mixtures to evaluate to what extent the nature of the side chains influences the self-assembly properties of the BiPy-BTA derivatives. The results are summarized in Figure 8 and Tables S2 and S4 (Supporting Information).

In all three studies, the general features are similar to those described for **1** in IPA–H_2O. An LCST transition is observed when the cosolvent content is below ϕ_{min} in all samples. The

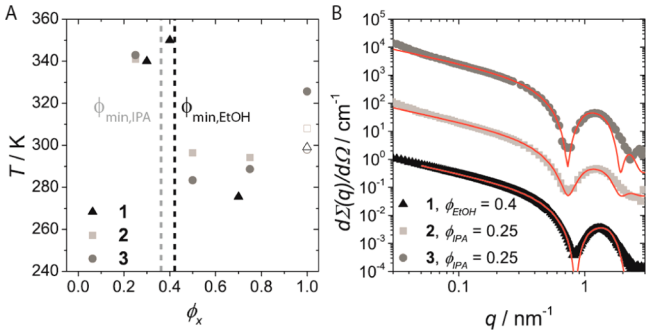

Figure 8. (A) Transition temperature (T_m or LCST) for **1** in EtOH–H_2O at $c = 3 \times 10^{-5}$ M and **2** and **3** in IPA–H_2O mixtures at $c = 3 \times 10^{-4}$ M. (B) SAXS profiles for **1** in EtOH–H_2O and **2** and **3** in IPA–H_2O mixtures at $c = 3 \times 10^{-4}$ M and $T = 20$ °C (data is offset by a factor of 10^2 (**2**) and 10^4 (**3**) for clarity).

LCSTs are at slightly higher temperatures (340–350 K) as compared to compound **1** in IPA–H_2O (335 K). Alternatively, if the solvent composition is between ϕ_{min} and ϕ_{max}, we observe a sigmoidal temperature-dependence of the CD effect, indicative of regime II behavior. Whereas in a 1:1 mixture the T_m of compound **1** in EtOH–H_2O (276 K) is similar to that in IPA–H_2O (278 K), the T_m for compounds **2** and **3** in IPA–H_2O are shifted to higher temperatures of 285 K and 295 K, respectively (Figure 8A and Figure S1B, Supporting Information).

In pure ethanol and isopropanol, all compounds show a sigmoidal temperature-dependence, indicative for regime III behavior. The T_m in regime III is similar for **2** at 326 K as compared to compound **1** in IPA where it was 328 K. For compound **3**, T_m was not within the experimentally accessible temperature range and exceeds 333 K. Next to this isodesmic self-assembly, at lower temperatures a second transition (T_2) at ca. 300–310 K is observed which coincides with the appearance of linear dichroism in the sample (Figure 8A). This indicates that at these temperatures aggregates are formed, which are sufficiently long to align within the sample.

The shape and size of the structures obtained for **1** in EtOH–H_2O, **2** in IPA–H_2O, and **3** in IPA–H_2O were characterized by SAXS. The results are very similar to those obtained for **1** in IPA–H_2O. Form factor fits reveal core–shell cylinder structures under all conditions at 20 °C (Figure 8B). The aggregate cross-section dimensions are similar to those of compound **1** in IPA–H_2O mixtures, having a core radius of ca. 1.5 nm and an outer radius of ca. 3.5 nm (Table S4, Supporting Information). This can be readily explained, as the cross-sectional size of the self-assembled structures is determined by the size of the amphiphilic BiPy-BTA discotic molecules, which is similar for all compounds. The length of the aggregates is not attainable in most scattering profiles.

A Phase Diagram. The previous observations can be summarized into the generalized phase diagram depicted in Figure 9. In this phase diagram, there are $\phi_{cosolvent}$-dependent

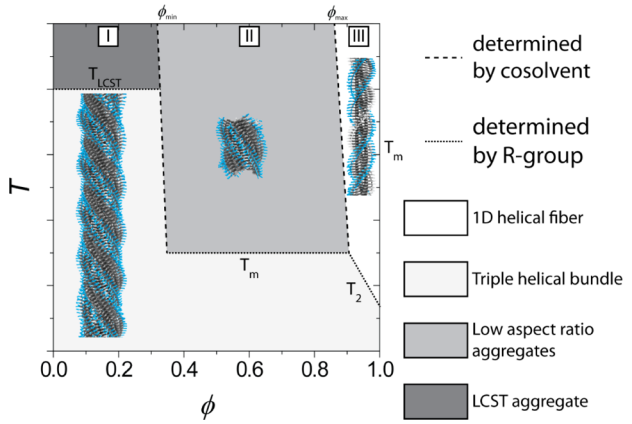

Figure 9. Generalized phase diagram of amphiphilic BiPy-BTA derivatives in alcohol–water mixtures.

boundaries between different aggregate structures linked to the positions of ϕ_{min} and ϕ_{max}. Below ϕ_{max}, hydrophobic interactions lead to bundle formation of the amphiphilic discotics while above ϕ_{max}, there is no driving force for this lateral association. In the intermediate regime the hydrophobic domains aggregate, but elongation into long, triple helical fibers occurs only below a certain temperature.

dx.doi.org/10.1021/ja4104183 | J. Am. Chem. Soc. 2014, 136, 336–343

There are also temperature-dependent boundaries between different aggregate structures. The LCST transition in regime I is weakly dependent on the nature of the cosolvent and the side-chain substitution. The temperature-dependent boundaries in regimes II and III are determined to a large extent by the nature of the side chains of the compound (R^1 and R^2). The transition temperature (T_m) for compound **1** in regime II is virtually the same in isopropanol and ethanol. On the other hand, T_m is higher for compound **3** than for compound **1**, indicating that the potential for packing/crystallization of the aliphatic side chains is important. This effect is also observed in mixing experiments of compounds **1** and **3** in pure isopropanol. Here we find a gradual, linear decrease of the T_2 transition temperature upon addition of **1** to a solution of **2** (Figure S2, Supporting Information). This indicates that disrupting the side-chain packing by mixing in a branched aliphatic side chain reduces the tendency of the aggregates to bundle.

It is noteworthy that the phase behavior of amphiphilic synthetic polymers and amphiphilic self-assembled structures is so similar in water−cosolvent mixtures. Whereas a full explanation of the observed phase behavior is not trivial, it is clearly related to the properties of the solvent mixture itself. Recent progress in the study of these complex water−cosolvent mixtures has revealed that even though they are macroscopically mixed, they phase separate at the nanoscopic level.[58−60] This could be the underlying mechanism for the phase behavior observed in these systems. The amphiphilic (small) molecules present in these complex mixtures "feel" the phase separation of the amphiphilic cosolvents and adapt their structure to accommodate this.

CONCLUSIONS

We are able to rationally design molecules that by means of $\pi-\pi$ stacking and hydrophobic interactions self-assemble into triple helical fibers. The morphology of aggregates of **1**−**3** can be tuned by the properties of the solvent mixture itself. The correlation between solvent composition and LCST behavior of temperature-sensitive polymers and supramolecular aggregates has been observed previously by various groups,[61−64] but Trappe and co-workers first noted the correlation with solvent thermodynamics, that is, the excess enthalpy of mixing, ΔH_{mix}^{E} and ϕ_{min} for thermo-sensitive polymers and proteins.[50] Herein we demonstrate that supramolecular polymers behave in a highly similar fashion. We report two morphological transitions that are coincident with the minima and maxima in ΔH_{mix}^{E} with $\phi_{I\rightarrow II} \sim \phi_{min}$ and $\phi_{II\rightarrow III} \sim \phi_{max}$. To the best of our knowledge, no such correlation has previously been reported for (supramolecular) polymers. A possible explanation could be the persistence of $\pi-\pi$ stacking up to $\phi_{IPA} = 1$ whereas the hydrophobic effect gradually disappears.

Solvent-driven morphological transitions may dominate supramolecular self-assembly in many aqueous cosolvent mixtures.[65−67] For example, George and co-workers studied the self-assembly of a coronene bisimide amphiphile in water−tetrahydrofuran mixtures and observed three self-assembly regimes.[68] The boundaries between these seem to correlate well with the ΔH_{mix}^{E} of the water−THF mixture.

In summary, the nanostructures obtained upon self-assembly in water can be greatly influenced by the preparation method. Frequently such samples are prepared by direct injection into water of solutions of small self-assembling units in a "good" solvent such as an alcohol or THF.[38,66,69−71] Understanding how the solvent composition influences the aggregate structures could help us understand the pathways by which the final structures in water are formed. Therefore, further investigation of this solvent effect and elucidating the mechanism behind it are crucially important to enable full control over hierarchical aggregation processes.

ASSOCIATED CONTENT

Supporting Information

Synthetic procedures, experimental details, spectroscopic SAXS and cryo-TEM data, equations used, and derived parameters. This material is available free of charge via the Internet at http://pubs.acs.org.

AUTHOR INFORMATION

Corresponding Authors

a.palmans@tue.nl;
e.w.meijer@tue.nl

Notes

The authors declare no competing financial interest.

ACKNOWLEDGMENTS

This work is financed by The Netherlands Organisation for Scientific Research (NWO - TOP grant: 10007851), the Dutch Ministry of Education, Culture and Science (Gravity program 024.001.035), and NRSC-C. I.K.V. is grateful for financial support from The Netherlands Organization for Scientific research (NWO - VENI grant: 700.10.406) and the European Union through the Marie Curie 5 Fellowship program FP7-PEOPLE-2011-CIG (contract no. 293788). The authors thank Koen Pieterse and Pol Besenius for their initial efforts on coiled-coil formation and Veronique Trappe for the helpful discussions. Part of this work is based on experiments performed at the ID2 High Brilliance Beamline at the European Synchrotron Radiation Facility (ESRF) in Grenoble. We also thank Dr. Narayanan Theyencheri for his assistance.

REFERENCES

(1) Aida, T.; Meijer, E. W.; Stupp, S. I. *Science* **2012**, *335*, 813.
(2) Kumar, S. *Chem. Soc. Rev.* **2006**, *35*, 83.
(3) Kato, T.; Mizoshita, N.; Kishimoto, K. *Angew. Chem., Int. Ed.* **2006**, *45*, 38.
(4) Elemans, J. A. A. W.; van Hameren, R.; Nolte, R. J. M.; Rowan, A. E. *Adv. Mater.* **2006**, *18*, 1251.
(5) Mart, R. J.; Osborne, R. D.; Stevens, M. M.; Ulijn, R. V. *Soft Matter* **2006**, *2*, 822.
(6) Hodges, R. S. *Curr. Biol.* **1992**, *2*, 122.
(7) Ebashi, S.; Ohtsuki, I.; Nitanai, Y.; Minakata, S.; Maeda, K.; Oda, N.; Maeda, Y. In *Regulatory Mechanisms of Striated Muscle Contraction*; Springer: Japan, 2007; Vol. *592*, p 137.
(8) Houston, M. E.; Campbell, A. P.; Lix, B.; Kay, C. M.; Sykes, B. D.; Hodges, R. S. *Biochemistry* **1996**, *35*, 10041.
(9) Bhattacharjee, A.; Bansal, M. *IUBMB Life* **2005**, *57*, 161.
(10) Ferrand, Y.; Gan, Q.; Kauffmann, B.; Jiang, H.; Huc, I. *Angew. Chem., Int Ed.* **2011**, *50*, 7572.
(11) Gan, Q.; Ferrand, Y.; Chandramouli, N.; Kauffmann, B.; Aube, C.; Dubreuil, D.; Huc, I. *J. Am. Chem. Soc.* **2012**, *134*, 15656.
(12) Yamada, H.; Furusho, Y.; Yashima, E. *J. Am. Chem. Soc.* **2012**, *134*, 7250.
(13) Hasenknopf, B.; Lehn, J. M.; Baum, G.; Fenske, D. *Proc. Natl. Acad. Sci. U.S.A.* **1996**, *93*, 1397.
(14) Tanaka, Y.; Katagiri, H.; Furusho, Y.; Yashima, E. *Angew. Chem., Int Ed.* **2005**, *44*, 3867.
(15) Peterca, M.; Percec, V.; Imam, M. R.; Leowanawat, P.; Morimitsu, K.; Heiney, P. A. *J. Am. Chem. Soc.* **2008**, *130*, 14840.

(16) Goto, H.; Furusho, Y.; Yashima, E. *J. Am. Chem. Soc.* **2007**, *129*, 9168.
(17) Goto, H.; Furusho, Y.; Miwa, K.; Yashima, E. *J. Am. Chem. Soc.* **2009**, *131*, 4710.
(18) Gan, Q.; Bao, C. Y.; Kauffmann, B.; Grelard, A.; Xiang, J. F.; Liu, S. H.; Huc, I.; Jiang, H. *Angew. Chem., Int Ed.* **2008**, *47*, 1715.
(19) Ferrand, Y.; Kendhale, A. M.; Garric, J.; Kauffmann, B.; Huc, I. *Angew. Chem., Int Ed.* **2010**, *49*, 1778.
(20) Berl, V.; Huc, I.; Khoury, R. G.; Krische, M. J.; Lehn, J. M. *Nature* **2000**, *407*, 720.
(21) Mateos-Timoneda, M. A.; Kerckhoffs, J.; Reinhoudt, D. N.; Crego-Calama, M. *Org. Biomol. Chem.* **2007**, *5*, 447.
(22) Aggeli, A.; Bell, M.; Carrick, L. M.; Fishwick, C. W. G.; Harding, R.; Mawer, P. J.; Radford, S. E.; Strong, A. E.; Boden, N. *J. Am. Chem. Soc.* **2003**, *125*, 9619.
(23) Chen, X.-M.; Liu, G.-F. *Chem.—Eur. J.* **2002**, *8*, 4811.
(24) Zubarev, E. R.; Pralle, M. U.; Sone, E. D.; Stupp, S. I. *J. Am. Chem. Soc.* **2001**, *123*, 4105.
(25) Taylor, P. N.; Anderson, H. L. *J. Am. Chem. Soc.* **1999**, *121*, 11538.
(26) Mamula, O.; von Zelewsky, A.; Bark, T.; Bernardinelli, G. *Angew. Chem., Int. Ed.* **1999**, *38*, 2945.
(27) Engelkamp, H.; Middelbeek, S.; J. M., R.; Nolte. *Science* **1999**, *284*, 785.
(28) Tikhomirov, G.; Yamazaki, T.; Kovalenko, A.; Fenniri, H. *Langmuir* **2008**, *24*, 4447.
(29) Li, J. X.; Wisner, J. A.; Jennings, M. C. *Org. Lett.* **2007**, *9*, 3267.
(30) Goto, H.; Furusho, Y.; Yashima, E. *J. Am. Chem. Soc.* **2007**, *129*, 109.
(31) Goto, H.; Katagiri, H.; Furusho, Y.; Yashima, E. *J. Am. Chem. Soc.* **2006**, *128*, 7176.
(32) Besenius, P.; Portale, G.; Bomans, P. H. H.; Janssen, H. M.; Palmans, A. R. A.; Meijer, E. W. *Proc. Natl. Acad. Sci. U.S.A.* **2010**, *107*, 17888.
(33) Leenders, C. M. A.; Albertazzi, L.; Mes, T.; Koenigs, M. M. E.; Palmans, A. R. A.; Meijer, E. W. *Chem. Commun.* **2012**, *49*, 1963.
(34) Brizard, A.; Stuart, M.; van Bommel, K.; Friggeri, A.; de Jong, M.; van Esch, J. *Angew. Chem., Int. Ed.* **2008**, *47*, 2063.
(35) von Groning, M.; de Feijter, I.; Stuart, M. C. A.; Voets, I. K.; Besenius, P. *J. Mater. Chem. B* **2013**, *1*, 2008.
(36) Bae, J.; Choi, J.-H.; Yoo, Y.-S.; Oh, N.-K.; Kim, B.-S.; Lee, M. *J. Am. Chem. Soc.* **2005**, *127*, 9668.
(37) Hermans, T. M.; BroerenMaarten, A. C.; Gomopoulos, N.; van der, S.; van GenderenMarcel, H. P.; SommerdijkNico, A. J. M.; Fytas, G.; Meijer, E. W. *Nat. Nano* **2009**, *4*, 721.
(38) Hill, J. P.; Jin, W.; Kosaka, A.; Fukushima, T.; Ichihara, H.; Shimomura, T.; Ito, K.; Hashizume, T.; Ishii, N.; Aida, T. *Science* **2004**, *304*, 1481.
(39) Boekhoven, J.; van Rijn, P.; Brizard, A. M.; Stuart, M. C. A.; van Esch, J. H. *Chem. Commun.* **2010**, *46*, 3490.
(40) Hartgerink, J. D.; Beniash, E.; Stupp, S. I. *Science* **2001**, *294*, 1684.
(41) Shao, H.; Gao, M.; Kim, S. H.; Jaroniec, C. P.; Parquette, J. R. *Chem.—Eur. J.* **2011**, *17*, 12882.
(42) Marsden, H. R.; Korobko, A. V.; van Leeuwen, E. N. M.; Pouget, E. M.; Veen, S. J.; Sommerdijk, N. A. J. M.; Kros, A. *J. Am. Chem. Soc.* **2008**, *130*, 9386.
(43) Danila, I.; Riobé, F.; Piron, F.; Puigmartí-Luis, J.; Wallis, J. D.; Linares, M.; Ågren, H.; Beljonne, D.; Amabilino, D. B.; Avarvari, N. *J. Am. Chem. Soc.* **2011**, *133*, 8344.
(44) Brunsveld, L.; Lohmeijer, B. G. G.; Vekemans, J. A. J. M.; Meijer, E. W. *Chem. Commun.* **2000**, 2305.
(45) Brunsveld, L.; Zhang, H.; Glasbeek, M.; Vekemans, J. A. J. M.; Meijer, E. W. *J. Am. Chem. Soc.* **2000**, *122*, 6175.
(46) Palmans, A. R. A.; Vekemans, J. A. J. M.; Havinga, E. E.; Meijer, E. W. *Angew. Chem., Int. Ed.* **1997**, *36*, 2648.
(47) Gillissen, M. A. J.; Hoeben, T. T.; Spiering, A. J. H.; Vekemans, J. A. J. M.; Palmans, A. R. A.; Meijer, E. W. *Isr. J. Chem.* **2011**, *51*, 1118.
(48) van Houtem, M. H. C. J.; Benaskar, F.; Fitie, C. F. C.; Martin-Rapun, R.; Vekemans, J. A. J. M.; Meijer, E. W. *Org. Biomol. Chem.* **2012**, *10*, 5898.
(49) van Houtem, M. H. C. J.; Martín-Rapún, R.; Vekemans, J. A. J. M.; Meijer, E. W. *Chem.—Eur. J.* **2010**, *16*, 2258.
(50) Trappe, V. Hydrophobic hydration: a matter of the mean energetics of water. Personal communication.
(51) Roosma, J.; Mes, T.; Leclère, P.; Palmans, A. R. A.; Meijer, E. W. *J. Am. Chem. Soc.* **2008**, *130*, 1120.
(52) Devos, A.; Remion, J.; Frisque-Hesbain, A.-M.; Colens, A.; Ghosez, L. *J. Chem. Soc., Chem. Commun.* **1979**, 1180.
(53) Smulders, M. M. J.; Nieuwenhuizen, M. M. L.; de Greef, T. F. A.; van der Schoot, P.; Schenning, A. P. H. J.; Meijer, E. W. *Chem.—Eur. J.* **2010**, *16*, 362.
(54) Glatter, O. In *Neutrons, X-rays and Light: Scattering Methods Applied to Soft Condensed Matter; The Inverse Scattering Problem in Small-Angle Scattering*; Lindner, P., Zemb, T., Eds.; Elsevier: Amsterdam, 2002; p 73.
(55) Franks, F.; Ives, D. J. G. *Q. Rev. Chem. Soc.* **1966**, *20*, 1.
(56) Katayama, T. *Kagaku Kogaku Ronbun.* **1962**, *26*, 361.
(57) Lama, R. F.; Lu, B. C. Y. *J. Chem. Eng. Data* **1965**, *10*, 216.
(58) Dixit, S.; Crain, J.; Poon, W. C. K.; Finney, J. L.; Soper, A. K. *Nature* **2002**, *416*, 829.
(59) Nakada, M.; Maruyama, K.; Yamamuro, O.; Misawa, M. *J. Chem. Phys.* **2009**, *130*, 074503.
(60) Takamuku, T.; Kumai, T.; Yoshida, K.; Otomo, T.; Yamaguchi, T. *J. Phys. Chem. A* **2005**, *109*, 7667.
(61) Betancourt, J. E.; Rivera, J. M. *J. Am. Chem. Soc.* **2009**, *131*, 16666.
(62) Richards, G. J.; Labuta, J.; Hill, J. P.; Mori, T.; Ariga, K. *J. Phys. Chem. Lett.* **2010**, *1*, 1336.
(63) Costa, R. O. R.; Freitas, R. F. S. *Polymer* **2002**, *43*, 5879.
(64) Schild, H. G.; Muthukumar, M.; Tirrell, D. A. *Macromolecules* **1991**, *24*, 948.
(65) Boekhoven, J.; Brizard, A. M.; van Rijn, P.; Stuart, M. C. A.; Eelkema, R.; van Esch, J. H. *Angew. Chem., Int. Ed.* **2011**, *50*, 12285.
(66) Che, Y.; Datar, A.; Balakrishnan, K.; Zang, L. *J. Am. Chem. Soc.* **2007**, *129*, 7234.
(67) Yang, Y.; Suzuki, M.; Owa, S.; Shirai, H.; Hanabusa, K. *J. Mater. Chem.* **2006**, *16*, 1644.
(68) Rao, K. V.; George, S. J. *Org. Lett.* **2010**, *12*, 2656.
(69) Huang, J.; Bonduelle, C.; Thévenot, J.; Lecommandoux, S.; Heise, A. *J. Am. Chem. Soc.* **2011**, *134*, 119.
(70) Chaudhary, N.; Singh, S.; Nagaraj, R. *J. Pept. Sci.* **2009**, *15*, 675.
(71) Stevens, A. L.; Kaeser, A.; Schenning, A. P. H. J.; Herz, L. M. *ACS Nano* **2012**, *6*, 4777.